Eur. Phys. J. Special Topics **224**, 3379–3392 (2015)

DOI: 10.1140/epjst/e2015-50021-3

THE EUROPEAN PHYSICAL JOURNAL SPECIAL TOPICS

Regular Article

Free vibration analysis of a robotic fish based on a continuous and non-uniform flexible backbone with distributed masses

W. Coral[1,2,a], C. Rossi[2], and O.M. Curet[3]

[1] Universidad Politécnica de Madrid, Madrid, Spain
[2] Centre for Automation and Robotics (CAR) UPM-CSIC, Madrid, Spain
[3] Department of Ocean and Mechanical Engineering, Florida Atlantic University (FAU), Boca Raton, USA

Received 7 March 2015 / Received in final form 2 November 2015
Published online 15 December 2015

Abstract. This paper presents a Differential Quadrature Element Method for free transverse vibration of a robotic fish based on a continuous and non-uniform flexible backbone with distributed masses (fish ribs). The proposed method is based on the theory of a Timoshenko cantilever beam. The effects of the masses (number, magnitude and position) on the value of natural frequencies are investigated. Governing equations, compatibility and boundary conditions are formulated according to the Differential Quadrature rules. The convergence, efficiency and accuracy are compared to other analytical solution proposed in the literature. Moreover, the proposed method has been validate against the physical prototype of a flexible fish backbone. The main advantages of this method, compared to the exact solutions available in the literature are twofold: first, smaller computational cost and second, it allows analysing the free vibration in beams whose section is an arbitrary function, which is normally difficult or even impossible with other analytical methods.

Nomenclature

x Global Spatial Coordinate
ξ Dimensionless Global Spatial Coordinate
$x^{(i)}$ Local Spatial Coordinate of Element i
$\zeta^{(i)}$ Dimensionless Local Spatial Coordinate of Element i
L Total Length of the Beam (m)
t Time (s)
$w(x,t)$, $W(x)$ Transverse Displacement
$\psi(x,t)$, $\Psi(x)$ Rotation Angle Due to Bending (rad)
$W^{(i)}$ Transverse Displacement of Element i
$\Psi^{(i)}$ Rotation Due to Bending of Element i
$v^{(i)}$ Dimensionless Transverse Displacement of Element i

[a] e-mail: william.coral@gmail.com

$l^{(i)}$ Dimensionless Length of Element i
$A(x)$ Cross Sectional Area of the Beam
$I(x)$ Moment of Inertia About the Neutral Axis (kg*m^2)
A_0 Values of the Cross-Section at the Clamped Edge
I_0 Values of the Moment of Inertia at the Clamped Edge
k Shear Correction Factor
E Young's Modulus of Elasticity (GPa)
$G(x)$ Shear Modulus of Beam Material (GPa)
ϑ Poisson's Ratio
ρ Mass Density (kg/m^3)
ω Angular Natural Frequency of Vibration (rad/s)
λ Dimensionless Natural Frequency of Vibration
r Slender Ratio
N Number of Grid Points
$M^{(i)}$ Bending Moment in Element i
$V^{(i)}$ Transverse Force in Element i
α_i Dimensionless Value of the i^{th} Concentrated Attached Mass
$J(x)$ Mass Moment of Inertia of the Beam per Unit Length (kg*m^2)
$A(x)$ Cross Sectional Area of the Beam
$Q(x)$ Beam Shear Rigidity, $kG(x)A(x)$
m_i Translational Inertia of the i^{th} Concentrated Mass (kg)
s Elastic Section Modulus

1 Introduction

The literature of robotic fishes and bio-inspired robots has several examples of structures using flexible materials that bend to produce thrust, for maneuvering [4,18], and even for energy harvesting [2]. However, few works analyze the normal frequency of vibration of the flexible structures employed as a way to optimize energy consumption. This allows a relatively small force applied repeatedly to make the amplitude of the oscillating system become very large. The purpose of this work is to study the resonance in the structure and how to create a steady motion with low energy consumption. This to build robots with improved energy efficiency. Thus, we take into consideration a robotic fish composed of a flexible backbone made of polycarbonate, and a series of relatively heavy (i.e. whose weigh is non negligible) ribs (Fig. 1). The dynamic characteristics of systems with flexible components is a very important issue that allows the study of robots based on a jointless structure. Researchers have addressed the problem of vibration analysis of structures with distributed masses located at arbitrary positions using the Delta Dirac function [3], introducing the mass in the boundary conditions [12], using the Rayleigh-Ritz method [13] or analyzing the case of flexible structures carrying distributed mass along the structure (including a free end) [5,8,9,16]. In all such cases, the authors use the Bernoulli-Euller beam theory to model simple structures, which is reliable just for slender beams. In order to increase the accuracy and reliability (especially for the beams with low length-to-thickness ratio), for the natural frequencies of a Timoshenko beam with a central point mass, a coupled displacement field method has been proposed (see, e.g., [17]).

The Differential Quadrature Element Method (DQEM), provides a powerful numerical method to analyze the behavior (both static and dynamic) in structures with some discontinuities in loading, material properties or in its geometry. Thus, this method is applied to solve many problems especially in vibration analysis.

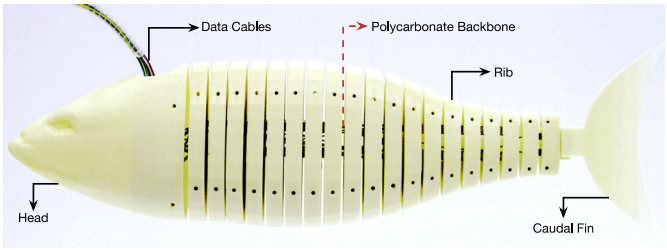

Fig. 1. The *robotic fish* prototype is composed of 19 ribs (excluding the head and the tail) made of 3D-printed ABS plastic that form the distributed masses.

1.1 Structure of the paper

In the following sections, we develop the method proposed to analyse the vibration of a non-uniform cantilever with distributed masses. Initially the method adopts the Differential Quadrature Element Method (DQEM, see Sect. 2) to get high accuracy for estimating the boundary conditions in more than two points. This method is more efficient than the one presented by Timoshenko for each section along the beam. In Sect. 3, governing equations are set for the free vibration using the Timoshenko beam. Section 4 shows the accuracy of the proposed DQEM, which is verified by comparison with the exact solutions of the uniform Timoshenko beam presented by other researchers. Finally, we present an application of the proposed method to our concrete case.

2 Differential quadrature method

The Differential quadrature (DQ) method allows expressing function derivatives in $x = x_i$ in terms of the value of function along the domain as:

$$\left.\frac{d^r f}{dx^r}\right|_{x=x_i} = \sum_{j=1}^{N} {A_{ij}}^{(r)} f_j, \tag{1}$$

where $A^{(r)}$ represents the weighting coefficient associated with the r^{th} order derivative and N the number of grid points [1]:

$${A_{ij}}^{(1)} = \begin{cases} \dfrac{\prod\limits_{\substack{m=1 \\ m\neq i,j}}^{N} (x_i - x_m)}{\prod\limits_{\substack{m=1 \\ m\neq j}}^{N} (x_j - x_m)}, & (i,j=1,2,3,\ldots N; i\neq j) \\ \sum\limits_{\substack{m=1 \\ m\neq i}}^{N} \frac{1}{(x_i - x_m)}, & (i=j=1,2,3,\ldots N) \end{cases} \tag{2}$$

$${A_{ij}}^{(r)} = \begin{cases} r\left({A^{(r-1)}}_{ii} {A^{(1)}}_{ij} - \frac{{A^{(r-1)}}_{ij}}{x_i - x_j}\right), & (i,j=1,2,3,\ldots N; i\neq j) \\ -\sum\limits_{\substack{m=1 \\ m\neq i}}^{N} {A^{(r)}}_{im}, & (i=j=1,2,3,\ldots N) \end{cases} \qquad 1<r\leq(N-1)$$

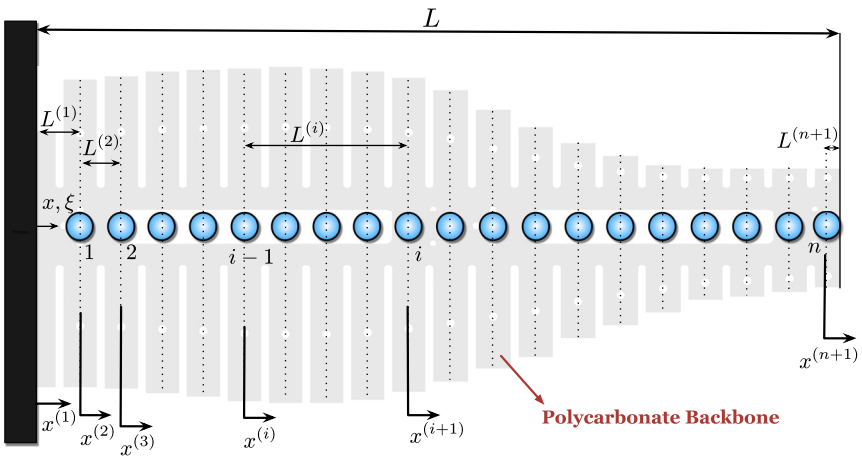

Fig. 2. Non-uniform *robotic fish* backbone with distributed masses.

Using a set of grid points (blue dots pot Fig. 2) following Gauss-Lobatto-Chebyshev points for interval $[0,1]$ we have

$$\overline{x}_i = \frac{1}{2}\left\{1-\cos\left[\frac{(i-1)\,\pi}{(N-1)}\right]\right\},\ (i=1,2,3,...N)\,. \tag{3}$$

This set of grid point shows the compression of the two end points in the interval $[0,1]$, providing in this way high accuracy for estimating the value of the derivative of the function at the boundary points.

3 Vibration analysis

3.1 Governing equations

Figure 2 shows the robotic fish backbone. Note that the mass of each rib is different and the backbone is non-uniform. The entire surface is modelled like a nonuniform cantilever Timoshenko beam. The Free Vibration governing equations for a Timoshenko beam [20] with distributed masses are written as[1]:

$$\begin{aligned}
&\frac{\partial}{\partial x}\left\{kGA\,(x)\left[\frac{\partial w\,(x,t)}{\partial x}-\psi\,(x,t)\right]\right\}-\rho A\,(x)\,\frac{\partial^2 w\,(x,t)}{\partial t^2}=0\\
&\frac{\partial}{\partial x}\left[EI\,(x)\,\frac{\partial \psi\,(x,t)}{\partial x}\right]+kGA\,(x)\left[\frac{\partial w\,(x,t)}{\partial x}-\psi\,(x,t)\right]-\rho I\,(x)\,\frac{\partial^2 w\,(x,t)}{\partial t^2}=0
\end{aligned} \tag{4}$$

where $w(x,t)$ is vertical displacement. The term k is introduced to take into account the geometry dependent distribution of the shear stress and depends on the shape of the section and the Poisson ratio of the material [10]. The displacement $w(x,t)$ and rotation due to bending $\psi(x,t)$ can be assumed as the product of the functions $W(x)$ and $\Psi(x)$ which only depend on the spatial coordinate x and a time dependent harmonic function, as:

$$w(x,t)=W(x)e^{i\omega t}\quad \psi(x,t)=\Psi(x)e^{i\omega t}. \tag{5}$$

[1] We don't use the Euler-Bernoulli beam theory because in this study the beam thickness is very small.

Substituting the Eq. (5) into the set of Eq. (4), we obtain

$$\frac{d^2W(x)}{dx^2}-\frac{d\Psi(x)}{dx}+\frac{1}{A^*(x)}\frac{dA^*(x)}{dx}\left[\frac{dW(x)}{dx}-\Psi(x)\right]+\frac{\rho\omega^2}{kG}W(x)=0,$$

$$\frac{EI_0}{kA_0G}\left[\frac{d^2\Psi(x)}{dx^2}+\frac{1}{I^*(x)}\frac{dI^*(x)}{dx}\frac{d\Psi(x)}{dx}\right]+\frac{A^*(x)}{I^*(x)}\left[\frac{dW(x)}{dx}-\Psi(x)\right]+\frac{\rho I_0\omega^2}{kA_0G}\Psi(x)=0. \tag{6}$$

The second moment of inertia and cross-sectional area are written in the following dimensionless form:

$$I^*(x)=\frac{I(x)}{I_0}\quad A^*(x)=\frac{A(x)}{A_0} \tag{7}$$

where I_0 and A_0 are values of the moment of inertia and cross-section at the clamped edge of the beam. For the i^{th} sub-beam, the set of Eqs. (6) are written as

$$\frac{d^2W^{(i)}(x^{(i)})}{d(x^{(i)})^2}-\frac{d\Psi^{(i)}(x^{(i)})}{dx^{(i)}}+\frac{1}{A^*(x)}\frac{dA^*(x)}{dx}\left[\frac{dW^{(i)}(x^{(i)})}{dx^{(i)}}-\Psi^{(i)}(x^{(i)})\right]+\frac{\rho\omega^2}{kG}W^{(i)}(x^i)=0$$

$$\frac{EI_0}{kA_0G}\left[\frac{d^2\Psi^{(i)}(x^{(i)})}{d(x^{(i)})^2}+\frac{1}{I^*(x)}\frac{dI^*(x)}{dx}\frac{d\Psi^{(i)}(x^{(i)})}{dx^{(i)}}\right]+\frac{A^*(x)}{I^*(x)}\left[\frac{dW^{(i)}(x^{(i)})}{dx^{(i)}}-\Psi^{(i)}(x^{(i)})\right]+\frac{\rho I_0\omega^2}{kA_0G}\Psi^{(i)}(x^{(i)})=0. \tag{8}$$

Introducing the dimensionless parameters:

$$\xi=\frac{x}{L}\quad\zeta^{(i)}=\frac{x^{(i)}}{L^{(i)}}\quad v^{(i)}=\frac{W^{(i)}}{L}\quad l^{(i)}=\frac{L^{(i)}}{L} \tag{9}$$

the set of Eqs (8) can be rewritten as

$$\left(\frac{1}{l^{(i)}}\right)^2\frac{d^2v^{(i)}\left(\zeta^{(i)}\right)}{d\left(\zeta^{(i)}\right)^2}-\left(\frac{1}{l^{(i)}}\right)\frac{d\Psi^{(i)}\left(\zeta^{(i)}\right)}{d\zeta^{(i)}}+\frac{1}{A^*(\xi)}\frac{dA^*(\xi)}{d\xi}\times\left[\left(\frac{1}{l^{(i)}}\right)\frac{dv^{(i)}\left(\zeta^{(i)}\right)}{d\zeta^{(i)}}-\Psi^{(i)}\left(\zeta^{(i)}\right)\right]+\lambda^4s^2v^{(i)}\left(\zeta^{(i)}\right)=0$$

$$s^2\left[\left(\frac{1}{l^{(i)}}\right)^2\frac{d^2\Psi^{(i)}\left(\zeta^{(i)}\right)}{d\left(\zeta^{(i)}\right)^2}+\frac{1}{I^*(\xi)}\frac{dI^*(\xi)}{d(\xi)}\left(\frac{1}{l^{(i)}}\right)\frac{d\Psi^{(i)}\left(\zeta^{(i)}\right)}{d\zeta^{(i)}}\right]+\frac{A^*(\xi)}{I^*(\xi)}\left[\left(\frac{1}{l^{(i)}}\right)\frac{dv^{(i)}\left(\zeta^{(i)}\right)}{d\zeta^{(i)}}-\Psi^{(i)}\left(\zeta^{(i)}\right)\right]+\lambda^4s^2r^2\Psi^{(i)}\left(\zeta^{(i)}\right)=0, \tag{10}$$

where

$$\lambda^4=\frac{\rho A_0L^4\omega^2}{EI_0},\quad s^2=\frac{EI_0}{kA_0GL^2}=\frac{2(1+v)}{k}r^2,\quad r^2=\frac{I_0}{A_0L^2}. \tag{11}$$

Assuming all grid points are the same for the sub-beams, then

$$\zeta^{(1)}=\zeta^{(2)}=\zeta^{(3)}=\ldots=\zeta^{(i)}=\ldots=\zeta^{(n+1)}=\zeta. \tag{12}$$

Thus, Eq. (10) can be simplified:

$$\left(\frac{1}{l^{(i)}}\right)^2\frac{d^2v^{(i)}(\zeta)}{d\zeta^2}-\left(\frac{1}{l^{(i)}}\right)\frac{d\Psi^{(i)}(\zeta)}{d\zeta}+\frac{1}{A^*(\xi)}\frac{dA^*(\xi)}{d\xi}\left[\left(\frac{1}{l^{(i)}}\right)\frac{dv^{(i)}(\zeta)}{d(\zeta)}-\Psi^{(i)}(\zeta)\right]+\lambda^4 s^2 v^{(i)}(\zeta)=0$$

$$s^2\left[\left(\frac{1}{l^{(i)}}\right)^2\frac{d^2\Psi^{(i)}(\zeta)}{d\zeta^2}+\frac{1}{I^*(\xi)}\frac{dI^*(\xi)}{d\xi}\left(\frac{1}{l^{(i)}}\right)\frac{d\Psi^{(i)}(\zeta)}{d\zeta}\right]+\frac{A^*(\xi)}{I^*(\xi)}\times\left[\left(\frac{1}{l^{(i)}}\right)\frac{dv^{(i)}(\zeta)}{d(\zeta)}-\Psi^{(i)}(\zeta)\right]+\lambda^4 s^2 r^2\Psi^{(i)}(\zeta)=0. \tag{13}$$

Furthermore, we introduce a modified form of the weighting coefficients of element i to simplify the differential quadrature (DQ) analogue equations defined as

$$[A]^{(i)}=\frac{[A]^{(i)}}{l^{(i)}}\quad [B]^{(i)}=\frac{[A]^{(i)}}{\left(l^{(i)}\right)^2}. \tag{14}$$

Using Eq. (14), we obtain for the governing set of equations of element i the DQ analogue:

$$\begin{aligned}&[B_{ve}]^{(i)}\{v\}^{(i)}-[A_{se}]^{(i)}\{\Psi\}^{(i)}+\lambda^4 s^2\{v\}^{(i)}=0,\\&[B_{se}]^{(i)}\{\Psi\}^{(i)}-[A_{ve}]^{(i)}\{v\}^{(i)}+\lambda^4 s^2 r^2\{\Psi\}^{(i)}=0\end{aligned} \tag{15}$$

where

$$\begin{aligned}&[B_{ve}]^{(i)}=[B]^{(i)}+\left[\frac{1}{A^*(\xi)}\frac{dA^*(\xi)}{d\xi}\right]^{(i)}[A]^{(i)}\qquad [A_{ve}]^{(i)}=\left[\frac{A^*(\xi)}{I^*(\xi)}\right]^{(i)}[A]^{(i)}\\&[B_{se}]^{(i)}=s^2\left([B]^{(i)}+\left[\frac{1}{I^*(\xi)}\frac{dI^*(\xi)}{d\xi}\right]^{(i)}[A]^{(i)}\right)-\left[\frac{A^*(\xi)}{I^*(\xi)}\right]^{(i)}\\&[A_{se}]^{(i)}=[A]^{(i)}+\left[\frac{1}{A^*(\xi)}\frac{dA^*(\xi)}{d\xi}\right]^{(i)}.\end{aligned} \tag{16}$$

In Eq. (16), the terms

$$\left[\frac{1}{A^*(\xi)}\frac{dA^*(\xi)}{d\xi}\right]^{(i)},\quad \left[\frac{A^*(\xi)}{I^*(\xi)}\right]^{(i)},\quad \left[\frac{1}{I^*(\xi)}\frac{dI^*(\xi)}{d\xi}\right]^{(i)}$$

are geometry-dependent diagonal matrices with values of the geometrical parameters. Now we can rewrite the motion Eqs. (15) for the domain points in order to eliminate the redundant equations ([6,7] and [15]) obtaining:

$$\begin{aligned}&\left[\overline{B_{ve}}\right]^{(i)}\{v\}^{(i)}-\left[\overline{A_{se}}\right]^{(i)}\{\Psi\}^{(i)}+\lambda^4 s^2\{\overline{v}\}^{(i)}=0\\&\left[\overline{B_{se}}\right]^{(i)}\{\Psi\}^{(i)}+\left[\overline{A_{ve}}\right]^{(i)}\{v\}^{(i)}+\lambda^4 s^2 r^2\left\{\overline{\Psi}\right\}^{(i)}=0\end{aligned} \tag{17}$$

where bar signs means truncated non-square matrices. Combining Eqs. (17):

$$[B_v]\{v\}-[A_s]\{\Psi\}+\lambda^4 s^2\{v\}_d=0\quad [B_s]\{\Psi\}+[A_v]\{v\}+\lambda^4 s^2 r^2\{\Psi\}_d=0 \tag{18}$$

where

$$\{v\}=\left\{\left\{\begin{Bmatrix} v_1^{(1)} \\ v_2^{(1)} \\ \cdot \\ \cdot \\ \cdot \\ v_{N-1}^{(1)} \\ v_N^{(1)} \end{Bmatrix}^T \begin{Bmatrix} v_1^{(2)} \\ v_2^{(2)} \\ \cdot \\ \cdot \\ \cdot \\ v_{N-1}^{(2)} \\ v_N^{(2)} \end{Bmatrix}^T \cdots \begin{Bmatrix} v_1^{(n+1)} \\ v_2^{(n+1)} \\ \cdot \\ \cdot \\ \cdot \\ v_{N-1}^{(n+1)} \\ v_N^{(n+1)} \end{Bmatrix}^T\right\}^T$$

$$\{\Psi\}=\left\{\left\{\begin{Bmatrix} \Psi_1^{(1)} \\ \Psi_2^{(1)} \\ \cdot \\ \cdot \\ \cdot \\ \Psi_{N-1}^{(1)} \\ \Psi_N^{(1)} \end{Bmatrix}^T \begin{Bmatrix} \Psi_1^{(2)} \\ \Psi_2^{(2)} \\ \cdot \\ \cdot \\ \cdot \\ \Psi_{N-1}^{(2)} \\ \Psi_N^{(2)} \end{Bmatrix}^T \cdots \begin{Bmatrix} \Psi_1^{(n+1)} \\ \Psi_2^{(n+1)} \\ \cdot \\ \cdot \\ \cdot \\ \Psi_{N-1}^{(n+1)} \\ \Psi_N^{(n+1)} \end{Bmatrix}^T\right\}^T$$

$$[B_v]=diag\left(\left[\overline{B_{ve}}\right]^{(1)}\left[\overline{B_{ve}}\right]^{(2)}\cdots\left[\overline{B_{ve}}\right]^{(n+1)}\right)\ [A_v]=diag\left(\left[\overline{A_{ve}}\right]^{(1)}\left[\overline{A_{ve}}\right]^{(2)}\cdots\left[\overline{A_{ve}}\right]^{(n+1)}\right)$$

$$[B_s]=diag\left(\left[\overline{B_{se}}\right]^{(1)}\left[\overline{B_{se}}\right]^{(2)}\cdots\left[\overline{B_{se}}\right]^{(n+1)}\right)\ [A_s]=diag\left(\left[\overline{A_{se}}\right]^{(1)}\left[\overline{A_{se}}\right]^{(2)}\cdots\left[\overline{A_{se}}\right]^{(n+1)}\right). \tag{19}$$

The "*diag*" operator provides the diagonal matrices. In order to separate the domain, boundary, adjacent displacement and rotation components, Eqs. (18) need to be rearranged [11]:

$$[B_v]_b\{v\}_b+[B_v]_d\{v\}_d+[B_v]_c\{v\}_c-[A_s]_b\{\Psi\}_b-[A_s]_d\{\Psi\}_d-[A_s]_c\{\Psi\}_c+\lambda^4 s^2\{v\}_d=0$$

$$[A_v]_b\{v\}_b+[A_v]_d\{v\}_d+[A_v]_c\{v\}_c+[B_s]_b\{\Psi\}_b+[B_s]_d\{\Psi\}_d+[B_s]_c\{\Psi\}_c+\lambda^4 s^2 r^2\{\Psi\}_d=0 \tag{20}$$

where

$$\{v\}_b=\begin{Bmatrix} \{v_1^{(1)}\} \\ \{v_N^{(n+1)}\} \end{Bmatrix}\ \{\Psi\}_b=\begin{Bmatrix} \{\Psi_1^{(1)}\} \\ \{\Psi_N^{(n+1)}\} \end{Bmatrix}$$

$$\{v\}_c=\left\{\{v_N^{(1)}\}\begin{Bmatrix} v_1^{(2)} \\ v_N^{(2)} \end{Bmatrix}^T\begin{Bmatrix} v_1^{(3)} \\ v_N^{(3)} \end{Bmatrix}^T\cdots\begin{Bmatrix} v_1^{(n)} \\ v_N^{(n)} \end{Bmatrix}^T\{v_1^{(n+1)}\}\right\}^T$$

$$\{\Psi\}_c=\left\{\{\Psi_N^{(1)}\}\begin{Bmatrix} \Psi_1^{(2)} \\ \Psi_N^{(2)} \end{Bmatrix}^T\begin{Bmatrix} \Psi_1^{(3)} \\ \Psi_N^{(3)} \end{Bmatrix}^T\cdots\begin{Bmatrix} \Psi_1^{(n)} \\ \Psi_N^{(n)} \end{Bmatrix}^T\{\Psi_1^{(n+1)}\}\right\}^T$$

$$\{v\}_d=\left\{\begin{Bmatrix} v_2^{(1)} \\ \vdots \\ v_{N-1}^{(1)} \end{Bmatrix}^T\begin{Bmatrix} v_2^{(2)} \\ \vdots \\ v_{N-1}^{(2)} \end{Bmatrix}^T\cdots\begin{Bmatrix} v_2^{(n+1)} \\ \vdots \\ v_{N-1}^{(n+1)} \end{Bmatrix}^T\right\}^T \tag{21}$$

$$\{\Psi\}_d=\left\{\begin{Bmatrix} \Psi_2^{(1)} \\ \vdots \\ \Psi_{N-1}^{(1)} \end{Bmatrix}^T\begin{Bmatrix} \Psi_2^{(2)} \\ \vdots \\ \Psi_{N-1}^{(2)} \end{Bmatrix}^T\cdots\begin{Bmatrix} \Psi_2^{(n+1)} \\ \vdots \\ \Psi_{N-1}^{(n+1)} \end{Bmatrix}^T\right\}^T$$

3.2 Compatibility conditions

We analyse the compatibility conditions that link the inertia and elasticity of the beam with the distributed masses.

Around each concentrated mass $[x_m^-, x_m^+]$ and neglecting the moment of inertia, the compatibility conditions are continuous in the vertical displacement and rotation. This due to the acceleration of distributed masses that produce a bending moment and a discontinuous transverse force.

$$\begin{aligned} &w\left(x_m^-,t\right)=w\left(x_m^+,t\right) \quad \psi\left(x_m^-,t\right)=\psi\left(x_m^+,t\right) \quad M\left(x_m^-,t\right)=M\left(x_m^+,t\right) \\ &V\left(x_m^-,t\right)-V\left(x_m^+,t\right)=m_i\frac{\partial^2 w(x,t)}{\partial t^2} \end{aligned} \tag{22}$$

where m_i, M, V are the translational inertia of the i^{th} concentrated mass, the bending moment and shear force respectively, which are presented for i^{th} sub-beam as [20]

$$M^{(i)}=EI\frac{d\Psi^{(i)}}{dx^{(i)}}=\frac{EI}{L}\frac{1}{l^{(i)}}\frac{d\Psi^{(i)}}{d\zeta} \quad V^{(i)}=kAG\left(\Psi^{(i)}-\frac{dW^{(i)}}{dx^{(i)}}\right)=kAG\left(\Psi^{(i)}-\frac{1}{l^{(i)}}\frac{d\Psi^{(i)}}{d\zeta}\right) \tag{23}$$

compatibility conditions can be expressed in the DQ form as

$$\begin{aligned} &v_N^{(i)}=v_1^{(i+1)} \quad \Psi_N^{(i)}=\Psi_1^{(i+1)} \quad \sum_{j=1}^{N}A_{1j}^{(i+1)}\Psi_j^{(i+1)}-\sum_{j=1}^{N}A_{Nj}^{(i)}\Psi_j^{(i)}=0 \\ &\sum_{j=1}^{N}A_{1j}^{(i+1)}v_j^{(i+1)}-\sum_{j=1}^{N}A_{Nj}^{(i)}v_j^{(i)}+\frac{\alpha_i s^2\lambda^4}{A^*\left(\xi_i\right)}v_N^{(i)}=0 \end{aligned} \tag{24}$$

we can define the dimensionless translational inertias of the i^{th} concentrated mass as

$$\alpha_i=\frac{m_i}{\rho A_0 L} \tag{25}$$

Eq. (24) can be rewritten in matrix form as

$$[Q_e]^{(i)}\begin{Bmatrix}\{v\}^{(i)}\\ \{v\}^{(i+1)}\end{Bmatrix}+\lambda^4[q_e]^{(i)}\begin{Bmatrix}\{v\}^{(i)}\\ \{v\}^{(i+1)}\end{Bmatrix}=\begin{Bmatrix}0\\0\end{Bmatrix} \quad [Q_e]^{(i)}\begin{Bmatrix}\{\Psi\}^{(i)}\\ \{\Psi\}^{(i+1)}\end{Bmatrix}=\begin{Bmatrix}0\\0\end{Bmatrix} \tag{26}$$

where

$$\begin{aligned} &[Q_e]_{jk}^{(i)}=\begin{cases}-\delta_{NK} & j=1,1\le k\le N\\ \delta_{(N+1)K} & j=1,N+1\le k\le 2N\\ -A_{Nk}^{(i)} & j=2,1\le k\le N\\ A_{1k}^{(i+1)} & j=2,N+1\le k\le 2N\end{cases} \\ &j=1,2 \\ &1\le k\le 2N \\ &[q_e]_{jk}^{(i)}=\begin{cases}\dfrac{\alpha_i s^2}{A^*\left(\xi_i\right)} & j=2,k=N\\ 0 & else\end{cases} \end{aligned} \tag{27}$$

Rewriting and composing a new Eq. (26) for all sub-beams,

$$[Q]\{v\}+\lambda^4[q]\{v\}=\{0\} \quad [Q]\{\Psi\}=\{0\} \tag{28}$$

where $[Q]$, $[q]$ are corresponding matrix that contains $[Q_e]^{(1)}$ to $[Q_e]^{(n+1)}$ and $[q_e]^{(1)}$ to $[q_e]^{(n+1)}$ respectively. Equation (26) may be rewritten and sectioned to separate

the components of domain, boundary, and adjacent displacement

$$\begin{aligned}&[Q]_b\{v\}_b+[Q]_d\{v\}_d+[Q]_c\{v\}_c+\lambda^4\left([q]_b\{v\}_b+[q]_d\{v\}_d+[q]_c\{v\}_c\right)=\{0\}\\&[Q_v]_b\{\Psi\}_b+[Q_v]_d\{\Psi\}_d+[Q_v]_c\{\Psi\}_c=\{0\}.\end{aligned}\tag{29}$$

From Eq. (27), it can be concluded that $[q]_b = [q]_d = 0$. Therefore, Eq. (29) can be summarized as

$$[Q]_b\{v\}_b+[Q]_d\{v\}_d+[Q]_c\{v\}_c+\lambda^4[q]_c\{v\}_c=\{0\}\tag{30}$$

$$\{\Psi\}_c=[J_b]\{\Psi\}_b+[J_d]\{\Psi\}_d\tag{31}$$

where

$$[J_b]=-[Q_v]_c^{-1}[Q_v]_b\quad[J_d]=-[Q_v]_c^{-1}[Q_v]_d.\tag{32}$$

Substituting Eq. (31) into Eq. (20)

$$\begin{aligned}&[B_v]_b\{v\}_b+[B_v]_d\{v\}_d+[B_v]_c\{v\}_c+[G_{sb}]\{\Psi\}_b+[G_{sd}]\{\Psi\}_d+\lambda^4s^2\{v\}_d=\{0\}\\&[A_v]_b\{v\}_b+[A_v]_d\{v\}_d+[A_v]_c\{v\}_c+[E_{sb}]\{\Psi\}_b+[E_{sd}]\{\Psi\}_d+\lambda^4s^2r^2\{\Psi\}_d=\{0\}\end{aligned}\tag{33}$$

where

$$\begin{aligned}&[G_{sb}]=[A_s]_b+[A_s]_c[J_b]\quad[G_{sd}]=[A_s]_d+[A_s]_c[J_d]\quad[E_{sb}]=[B_s]_b+[B_s]_c[J_b]\\&[E_{sd}]=[B_s]_d+[B_s]_c[J_d].\end{aligned}\tag{34}$$

3.3 Boundary conditions

The boundary conditions for a cantilever beam (robotic fish backbone) depicted in Fig. 2 can be considered as

$$W^{(1)}\big|_{x^{(1)}=0}=0\quad\psi^{(1)}\big|_{x^{(1)}=0}=0\quad V^{(n+1)}\big|_{x^{(n+1)}=L^{(n+1)}}=0\quad M^{(n+1)}\big|_{x^{(n+1)}=L^{(n+1)}}=0.\tag{35}$$

Equation (35) can be rewritten using Eq. (23) as

$$\Psi^{(1)}\big|_{x^{(1)}=0}=0\quad\frac{1}{l^{(i)}}\frac{d\Psi^{(n+1)}}{d\zeta}\Big|_{\zeta=1}=0\quad v^{(1)}\big|_{x^{(1)}=0}=0\quad\left(\frac{1}{l^{(i)}}\frac{d\Psi^{(n+1)}}{d\zeta}-\Psi^{(n+1)}\right)\Big|_{\zeta=1}=0.\tag{36}$$

In the DQ form, Eq. (36) can be indicated as

$$[m]\{\Psi\}=0\tag{37}$$

$$[m]\{v\}+[n]\{\Psi\}=\{0\}\tag{38}$$

where

$$\begin{aligned}&m_{jk}=\begin{cases}1 & j=k=1\\ A^{(n+1)}_{N(k-nN)} & j=2,nN+1\le k\le(n+1)N\\ 0 & else\end{cases}\\&j=1,2\\&1\le k\le(n+1)N\\&n_{jk}=\begin{cases}-1 & j=2,k=(n+1)N\\ 0 & else.\end{cases}\end{aligned}\tag{39}$$

Equations (37) and (38) can be rewritten and sectioned in order to separate the components (boundary, domain, adjacent displacement and rotation)

$$\begin{aligned}&[m]_b\{\Psi\}_b+[m]_d\{\Psi\}_d+[m]_c\{\Psi\}_c=\{0\}\\&[m]_b\{v\}_b+[m]_d\{v\}_d+[m]_c\{v\}_c+[n]_d\{\Psi\}_d+[n]_c\{\Psi\}_c=\{0\}.\end{aligned}\tag{40}$$

From Eq. (39), we know that $[n]_c = [n]_d = 0$; Hence, using Eq. (31), Eq. (40) we have

$$\{\Psi\}_b=[t]\{\Psi\}_d \quad \{v\}_b=-[m]_b^{-1}[m]_d^{-1}\{v\}_d-[m]_b^{-1}[m]_c^{-1}\{v\}_c-[m]_b^{-1}[n]_b[t]\{\Psi\}_d\tag{41}$$

where

$$[t]=-[r]_b^{-1}[r]_d \quad [r]_b=[m]_b+[m]_c[J_b] \quad [r]_b=[m]_d+[m]_c[J_d].\tag{42}$$

Replacing Eq. (41) into the set of Eqs. (20) and (30), a new set of equations is obtained:

$$[K]\begin{Bmatrix}\{v\}_d\\\{v\}_c\\\{\Psi\}_d\end{Bmatrix}=\lambda^4[M]\begin{Bmatrix}\{v\}_d\\\{v\}_c\\\{\Psi\}_d\end{Bmatrix}\tag{43}$$

where

$$[K]=\begin{bmatrix}[B_v]_d-[B_v]_b[m]_b^{-1}[m]_d & [B_v]_c-[B_v]_b[m]_b^{-1}[m]_c & [G_{sd}]+[G_{sb}][t]-[B_v]_b[m]_b^{-1}[n]_b[t]\\[Q]_d-[Q]_b[m]_b^{-1}[m]_d & [Q]_c-[Q]_b[m]_b^{-1}[m]_c & -[Q]_b[m]_b^{-1}[n]_b[t]\\[A_v]_d-[A_v]_b[m]_b^{-1}[m]_d & [A_v]_c-[A_v]_b[m]_b^{-1}[m]_c & [E_{sd}]+[E_{sb}][t]-[A_v]_b[m]_b^{-1}[n]_b[t]\end{bmatrix}$$

$$[M]=-\begin{bmatrix}s^2I_{(n+1)(N-2)*(n+1)(N-2)} & \{0\}_{(n+1)(N-2)*2n} & \{0\}_{(n+1)(N-2)*(n+1)(N-2)}\\\{0\}_{2n*(n+1)(N-2)} & [q]_c & \{0\}_{2n*(n+1)(N-2)}\\\{0\}_{(n+1)(N-2)*(n+1)(N-2)} & \{0\}_{(n+1)(N-2)*2n} & s^2r^2I_{(n+1)(N-2)*(n+1)(N-2)}\end{bmatrix}.\tag{44}$$

Using Eq. (44), we can determine the natural frequencies and corresponding mode shapes. The corresponding mode shapes can be completed using the Eqs. (31) and (41). It should be noted that the number of grid points affects the results. The number of grid points must be determined to satisfy the following relation for convergence of first n frequencies:

$$\left|\frac{\lambda_l{}^{(N)}-\lambda_l{}^{(N-1)}}{\lambda_l{}^{(N-1)}}\right|\leq\varepsilon \quad l=1,2,...n\tag{45}$$

where ε is considered as 0.01 in this study.

4 Experimental results

4.1 Numerical comparison

In order to assess the effectiveness of the proposed method, we have compared its accuracy with the exact solution obtained with the method proposed by Lee and Len [14].

We applied both methods to a cantilever Timoshenko beam with ($v = 0.25, k = 2/3$), an attached tip mass ($\alpha = 0.32$), beam cross-sectional properties $A = A_0(1 - 0.4\xi)$ and $I = I_0(1 - 0.4\xi)^3$ for a slenderness ratio r of 0.1 and 0.04 as shown in Table 1.

Table 1. Comparison between this method and the exact method proposed by [14] for the first three non-dimensional frequencies (λ^2).

Slenderness ratios r		0.04			0.1	
Modes of Vibration	1	2	3	1	2	3
Presented Method	2.117	13.42	36.11	1.997	10.69	24.34
Lee and Lin (1995)	2.099	13.55	36.76	2.015	11.07	25.63

(a) Robotic fish including a silicone-rubber-based skin

(b) Image acquisition scheme

Fig. 3. Experimental Setup.

4.2 Practical application

Our goal was to analyse the natural frequency in the robotic fish that we are developing, in order to optimise its energy efficiency. However, this analytical method can only be used for any kind of robots which are completely or partially based on a continuous and flexible structure. This also applies to robots whose structure is based on materials that work as actuators [21,22]. Therefore, we have applied our method to the physical prototype using the setup depicted in Fig. 3. The parameters modelling the robotic fish body as a conical Timoshenko beam where: slender ratio ($r = 1.03$), elastic section modulus ($s = 2.58$), diameter variation $d = d_0(1 - 0.5\xi)$ and uniformly spaced distributed masses ($\alpha = 1.3$). The number of distributed masses (n) are 19 this corresponds to the number of masses (ribs) in the robotic fish.

In order to analyse the behavior of the backbone, the tail was set to its initial position (Fig. 4a) and then released. Figure 4 shows the evolution of this movement. The settling time was 6 seconds. White marks in the tail were used to allow a particle tracking software (Tracker [23]) to find the free vibration response (Fig. 5a) and the experimental natural frequency (Fig. 5b), using a Canon EOS 7D camera with a 50mm f1.8 lens to capture the movement at 60 frames per second. The figure 5b was obtained by using the Fast Fourier Transform (FFT) that allows us to analyse a signal's spectrum with MATLAB®.

From the analysis of the images recorded, the natural frequency of the structure obtained experimentally was 2.1249 Hz.

5 Discussion and conclusions

In this work, we proposed the use of a theoretical model to find the natural frequency of a robotic fish with distributed masses along a flexible, continuous and non-uniform

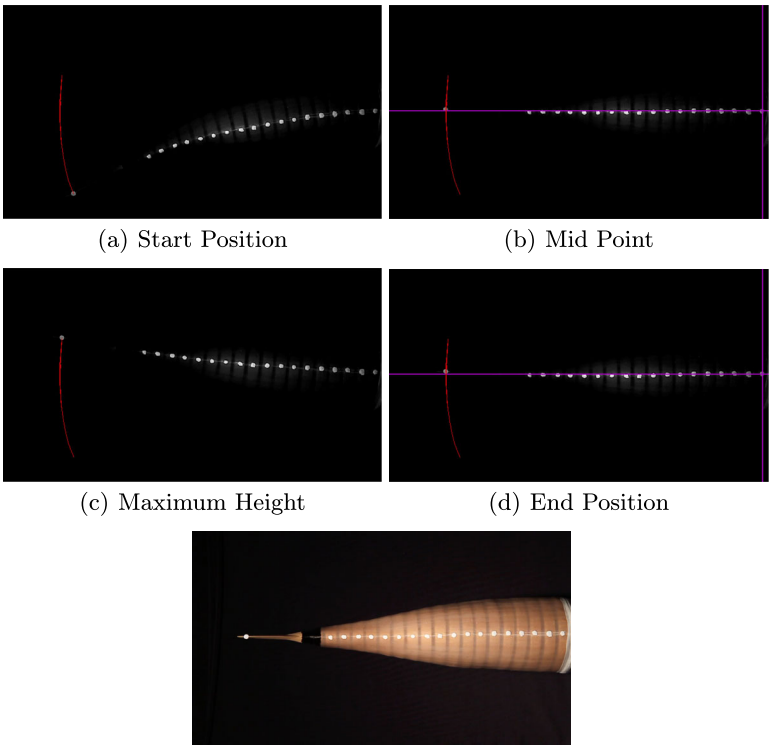

(a) Start Position (b) Mid Point

(c) Maximum Height (d) End Position

(e) Reference Fish View

Fig. 4. Free vibration analysis of the backbone. The white spots are the marks for the tracking, the red line is the trajectory of the tail.

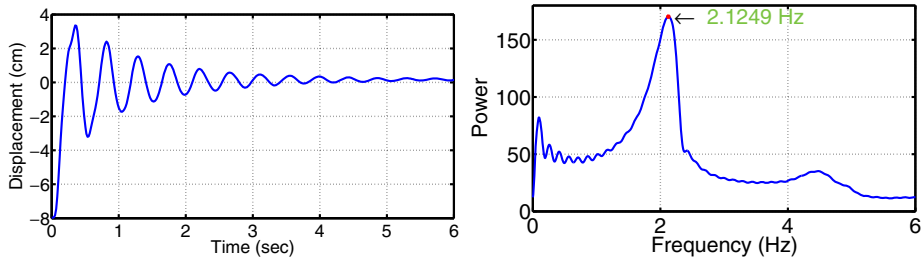

(a) Free Vibration (Displacement y axis) (b) Power Spectrum

Fig. 5. Experimental results. The natural frequency obtained was 2.1249 Hz.

backbone. The theoretical model proposed can be used for the beams with a large number of sections and capable of analyse the non-uniform beams with any variation in the cross section and moment of inertia. A comparison with an exact method for a set of cases where this could be applied assessed the goodness of the proposed method.

Comparing the data obtained experimentally for a physical prototype we could confirm that our method can effectively be used to analyse the free vibration in beams whose section is an arbitrary function, and with distributed masses. Also it can be observed the good accuracy for the proposed method.

Note the small variation of 0.2519 Hz between the theoretical value (1.873 Hz) and the one obtained experimentally (2.1249 Hz). This is due to the flexible skin, whose effect was not considered. The corresponding three modes for n=19 are depicted in

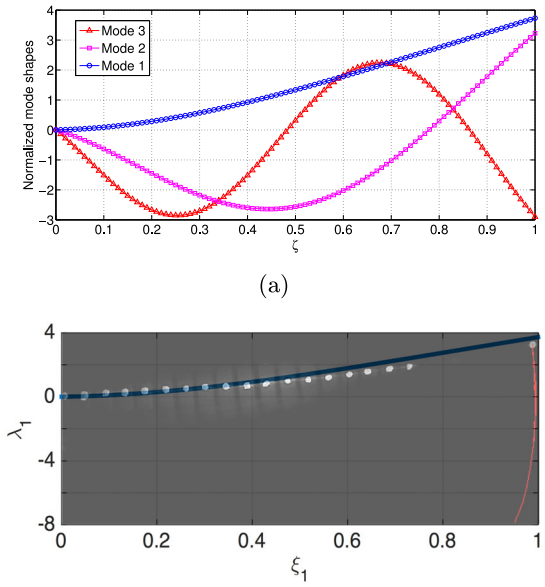

(a)

(b)

Fig. 6. (a) First three modes of robotic fish with nineteen equally spaced similar concentrated masses. (b) Robotic fish maximum height Fig. 5c vs. Mode 1 Fig. 6a.

Fig. 6a. The first frequency of the bean with concentrated masses versus the position of the robotic fish is plotted in Fig. 6b.

Adding the effects of the skin and hydrodynamics in the analytical model will be object of future work. However this can be made by using the inviscid fluid model of Chu [24] which its good accuracy has been demonstrated in comparison to experimental measurements [25]. The Chu's model relates the density of the fluid (ρ_{fluid}), the resonant frequencies in vacuum (ω_{vac}) and fluid (ω_{fluid}) and density (ρ), width (b) and thickness (h) of the beam. This can and has been successfully used to predict the resonant frequencies of cantilever beams of rectangular cross section immersed in viscous fluids. This still needs to be done.

The work of the first author has been funded by the Administrative Department of Science, Technology and Innovation (COLCIENCIAS) (grant call 568 2013) and COLFUTURO (grant call 2012) of Colombia. The authors acknowledge the support of the Robotics and Cybernetics Group and of Prof. R. Saltaren of the Centre for Automation and Robotics UPM-CSIC. This work has been co-funded by the RoboCity2030-III-CM project (Robotica aplicada a la mejora de la calidad de vida de los ciudadanos. fase III; S2013/MIT- 2748), funded by Programas de Actividades I+D en la Comunidad de Madrid and co-funded by Structural Funds of the EU.

References

1. C.W. Bert, M. Malik, Appl. Mech. Rev. **49**, 1 (1996)
2. Y. Cha, M. Verotti, H. Walcott, S. Peterson, M. Porfiri, Bioinspir. Biomimet. **8**, 3 (2013)
3. Y. Chen, J. Appl. Mech. **30**, 310 (1963)
4. W. Coral, et al., Smart Actuation and Sensing Systems – Recent Advances and Future Challenges. Chapter 3, SMA-Based Muscle-Like Actuation in Biologically Inspired Robots: A State of the Art Review (INTECH, 2012), p. 53

5. M.A. De Rosa, C. Franciosi, M.J. Maurizi, Comp. Struct. **58**, 1145 (1955)
6. H. Du,, M.K. Lim, N.R. Lin, Inter. J. Numer. Meth. Eng. **37**, 1881 (1994)
7. H. Du, M.K. Lim, N.R. Lin, J. Sound Vibr. **181**, 279 (1995)
8. M. Gurgoze, J. Sound Vibr. **96**, 461 (1984)
9. M. Gurgoze, J. Sound Vibr. **100**, 588 (1985)
10. T. Kaneko, J. Phys. D: Appl. Phys. **8**, 1928 (1975)
11. G. Karami, P. Malekzadeh, Comp. Meth. Appl. Mech. Eng. **191**, 3509 (2002)
12. P. Laura, M.J. Maurizi, J.L. Pombo, J. Sound Vibr. **41**, 397 (1975)
13. P. Laura, P.L. Verniere de Irassar, G.M. Ficcadenti, J. Sound Vibr. **86**, 279 (1983)
14. S.Y. Lee, S.M. Lin, J. Sound Vibr. **183**, 403 (1995)
15. R.M. Lin, M.K. Lim, H. Du, Comput. Struct. **53**, 993 (1994)
16. W.H. Liu, J.R. Wu, C.C. Huang, J. Sound Vibr. **122**, 193 (1988)
17. G.V. Rao, K.M. Saheb, G.R. Janardhan, J. Sound Vibr. **298**, 221 (2006)
18. C. Rossi, W. Coral, et al., Bioinspir. Biomimet. **6**, 15 (2011)
19. C. Rossi, W. Coral, et al., A Motor-less and Gear-less Bio-mimetic Robotic Fish Design, 2011 IEEE International Conference on Robotics and Automation (2011)
20. S. Timoshenko, D.H. Young, W. Weaver, Vibration problems in engineering (Wiley, New York, 1974)
21. M. Aureli, V. Kopman, M. Porfiri, Free-locomotion of underwater vehicles actuated by ionic polymer metal composites. IEEE/ASME Transactions on **15**(4), 603 (2010)
22. P. Phamduy, R. LeGrand, M. Porfiri, Robotics & Automation Magazine, IEEE **22**(1), 86 (2015)
23. Tracker, Video Analysis and Modelling Tool, `http://physlets.org/tracker/` (accessed September 10, 2015)
24. W.-H. Chu, Technical Report No. 2, DTMB, Contract NObs-86396(X), Southwest Research Institute (San Antonio, Texas, 1963)
25. U.S. Lindholm, D.D. Kana, W.-H. Chu, H.N. Abramson, J. Ship. Res. **9**, 11 (1965)